Journal of Power Sources 238 (2013) 469–477

Contents lists available at SciVerse ScienceDirect

Journal of Power Sources

journal homepage: www.elsevier.com/locate/jpowsour

Nanoindentation testing of separators for lithium-ion batteries

Ion C. Halalay*, Michael J. Lukitsch, Michael P. Balogh, Curtis A. Wong [1]

General Motors Global R&D, 30500 Mound Road, Warren, MI 48090-9055, USA

HIGHLIGHTS

- Nanoindentation determines the elastic modulus and the hardness of separators.
- Properties are probed on electrode active material particles length scales.
- Nanoindentation quantifies the in-plane uniformity of the mechanical properties.
- Improvement of mechanical properties by ceramics: 3× for modulus, 2× for hardness.
- The use of ceramics does not guarantee better mechanical properties in separators.

ARTICLE INFO

Article history:
Received 14 January 2013
Received in revised form
4 April 2013
Accepted 5 April 2013
Available online 24 April 2013

Keywords:
Separator
Microporous membrane
Nanoindentation
Elastic modulus
Hardness

ABSTRACT

We describe herein a method for quantifying and ranking the puncture resistance of lithium-ion battery separators, which can be used as a quality-control tool for determining the in-plane uniformity of their mechanical properties. Mechanical properties were probed over length scales comparable to the size of electrode active material particles. We determined the elastic modulus and hardness of four polymeric and four organic–inorganic composite separators through nanoindentation, and examined their morphology with scanning electron microscopy. Our results show that ceramic-enhanced separators can have improved mechanical properties compared to polymeric separators (3× increase in elastic modulus, 2× increase in hardness). Composite separators made of ultra-high molecular weight polyethylene and fumed alumina displayed the highest hardness. The results also indicate that the mechanical properties of ceramic-enhanced separators depend strongly on materials choices and processing conditions (in particular, their thermal history). Furthermore, inclusion of ceramics into a separator does not guarantee improved mechanical properties.

1. Introduction

Separators have a significant influence on the performance, safety, and cost of lithium-ion batteries (LIBs), and represent an essential component of any LIB with liquid electrolyte. In recent years it has become apparent that the mechanical integrity and dimensional stability of the separator can reduce the risk resulting from physical contact between electrodes in high energy high power LIBs. However, debate still exists regarding test procedures that best simulate an internal short and experiments that best quantify a separator's ability to prevent internal shorting.

An LIB separator is basically a porous stand-off placed between the negative and positive electrodes. Its two main functions are (i) to prevent a short circuit by direct contact between the electrodes and (ii) to allow ionic transport through the liquid contained in its open pores. The ideal separator has infinite electronic and zero ionic resistivity. While the former requirement is well approximated by polymers, ceramics and glasses (having an electronic resistivity ranging from 10^{12} to 10^{14} Ω cm), the latter is much less fulfilled, since the porosity cannot be 100%, so the resistance of the composite inter-electrode medium formed by the electrolyte and separator is 3–15 times higher than that of the liquid electrolyte occupying the same space.

In small commercial cells under abuse conditions the separator is required to shutdown the electric current flow at temperatures below those corresponding to thermal runaway [1]. Shutdown is produced through the collapse of pores due to melting of polyethylene, thus slowing down and eventually stopping the ion flow between the electrodes. While, in principle, shutdown through pore collapse should prevent thermal runaway, LIB field failures accompanied by exothermic events prove that shutdown does not guarantee thermal abuse tolerance. One possible cause for such field failures is small metal particles ingressing the battery during

* Corresponding author.
E-mail address: Ion.C.Halalay@gm.com (I.C. Halalay).
[1] Retired.

0378-7753/$ – see front matter © 2013 Elsevier B.V. All rights reserved.
http://dx.doi.org/10.1016/j.jpowsour.2013.04.036

fabrication and thus providing a direct shorting path between the battery after cutting through the separator. A metal fine will provide a shorting path even after the separator pores collapse, causing intense local heating. At this point residual stresses and the reduced mechanical properties at temperatures exceeding the polymer melting point lead to severe separator shrink-back. Since an LIB is hermetically sealed, local removal of the separator creates a virtual vacuum that will cause the electrodes to touch and produce a massive internal short circuit, which in turn leads to thermal runaway and battery failure ending with an energetic event.

The utility of shutdown has been called into question for large cells, as used for automotive transportation [2], where most mitigation measures for failure modes in which separator shutdown might play a role are taken at system level. Internal short-circuits in a LIB can have several causes: (i) dendrite growth; (ii) direct contact between the negative electrode and the aluminum current collector due to poor areal overlap between the separator and the electrodes, and (iii) conductive particles lodged in the inter-electrode spacing. Dendrite growth, caused by lithium plating on overcharge or copper plating on overdischarge, can be prevented through battery control strategies. Misalignment between the separator and the electrodes can be eliminated through improvements in cell design and better control of the manufacturing process. Battery failures due to internal short-circuits caused by lose conductive particles located the inter-electrode space cannot be mitigated by control strategies or battery design, and improvements in manufacturing can only reduce their occurrence rate.

There exist two distinct scenarios for cell shorting by conductive particles lodged in the inter-electrode spacing and, correspondingly, two material properties quantify a separator's ability to prevent it, depending on cell geometry. The electrodes of a LIB experience successive expansions and contractions during charge–discharge cycling. (1) In a *prismatic cell*, a trapped conducting particle experiences a periodically varying force perpendicular to the plane of the electrodes and will produce a short circuit after piercing through the separator. *Puncture resistance* is therefore the relevant material functionality. (2) In a *cylindrical cell*, successive expansions and contractions of the electrodes during prolonged charge–discharge cycling cause a periodic tangential motion of the electrodes. A metallic particle trapped in the inter-electrode space will therefore perform a see–saw motion and will cause a short-circuit after slicing through the separator. *Abrasion resistance* is now the relevant material functionality. The present work only quantifies the puncture resistance, through measurements of elastic modulus and hardness.

The ASTM F1306-90 test method [3], widely used at present in the battery industry for testing the puncture resistance of separators, prescribes the use of a hemispherical indenter with a 3.2 mm diameter and consists of recording the force applied to it as a function of penetration depth until reaching film breakthrough. The test was developed for the packaging industry and several objections can be raised about its applicability to battery separators. First, the ASTM test is strictly empirical and does not yield values for any material property. Its usefulness for engineering calculations and design is therefore limited. Second, the indenter diameters in this test exceed the separator thickness by 1–2 orders of magnitude. Microscopy reveals an inhomogeneity scale less than 0.1 mm in separators, due pores and, sometimes, inorganic fillers. Indenters with diameters greatly exceeding the separator thickness have therefore dubious utility for quantify the separator resistance to puncture by very small conductive particles. A third and more

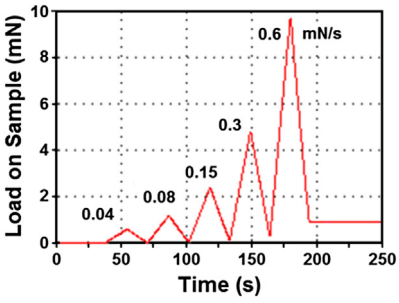

Fig. 1. Load on sample as a function of time, during the nanoindentation tests consisting of five load–unload cycles of increasing amplitude. Each load–unload segment ends at 10% of the maximum load reached during the respective segment.

Table 1
Properties of tested separators, as specified by their manufacturers.

No.	Polymeric material	Ceramic material & placement	Thickness, μm	Porosity, %	Notes
1	PP	N/A	25	55	–
2	PP	N/A	27	37	–
3	PP–PE–PP	N/A	21.5	50	–
4	PTFE	N/A	23	65	–
5	PET	$Al_2O_3 + SiO_2$ filler & coating	30	40	–
6	PP–PE–PP	Al_2O_3 coating	25	34	–
7	UHMWPE	Al_2O_3 filler	62	79	As-prepared
8	UHMWPE	Al_2O_3 filler	52	79	Heat treated

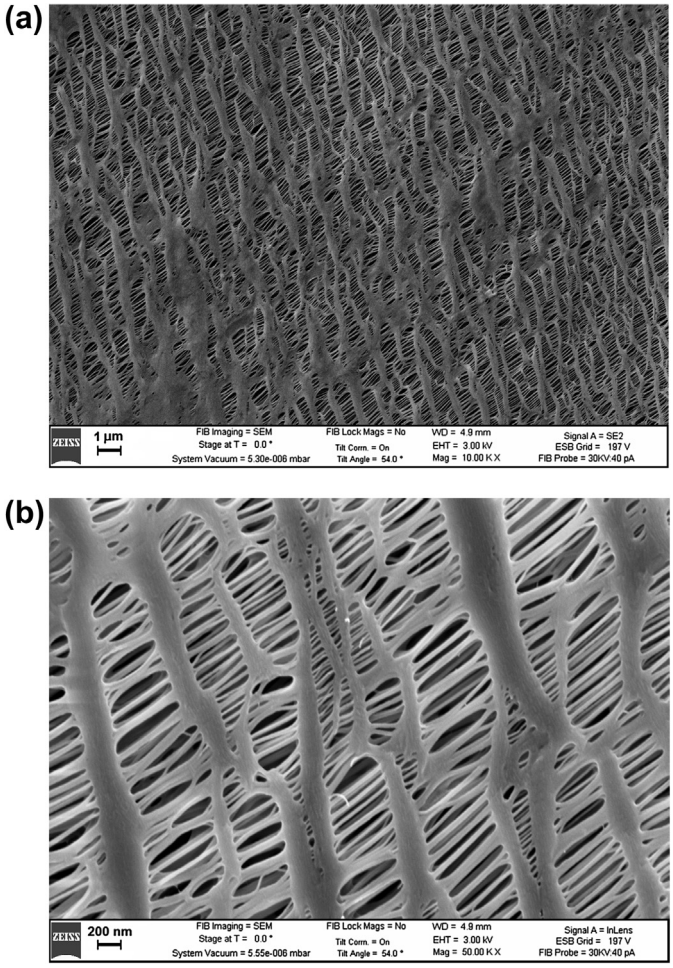

Fig. 2. SEM micrographs of the single layer PP1 separator: (a) surface at low magnification; (b) surface at high magnification.

pertinent objection stems from the test conditions prescribed by the ASTM method, since they do not replicate the mechanical constraints experienced by a separator inside a battery. The sample is clamped between two plates having a circular orifice placed coaxially with respect to each other, so the indenter exerts a shear force on it. On the other hand, the separator inside a battery is supported on both sides by electrode surfaces and so cannot experience any shear.

The questionable applicability of the ASTM test to separators has long been recognized by separator manufacturers. Celgard, in particular, developed a test for the so-called "*z*-direction strength" of a separator [4,5]. While this represents an improvement over the ASTM test, two objections come to mind. First, this test is strictly empirical, as it does not measure any mechanical property. Second, its results depend not only on separator properties, but also on active material particle size and surface roughness of the electrodes. Comparison of results from different laboratories is therefore difficult, if not meaningless.

Several recently published papers address the influence of separator mechanical properties on Li-ion battery performance [6–10]. They report on important issues such as the stress distribution in a separator during battery cycling [6], the influence of separator creep on battery capacity retention [9] and the relationship between strain in the separator and ionic transport [10]. However, in all these studies the separator is treated as a homogenous medium characterized by average mechanical properties [6–8] and measurement methods determine macroscopic averages [6,9,10], without any attempt to investigate the effect of inhomogeneity at mesoscopic and microscopic levels on separator properties or battery performance beyond the semi-empirical Bruggeman relationship [10]. Information regarding battery separator homogeneity is important, since homogeneity has a direct impact on the uniformity of the current distribution, and thus on battery performance and durability.

Nanoindentation, on the other hand, determines the mechanical properties (elastic modulus and hardness) [11,12] of separators on length scales comparable to typical sizes of active material particles in battery electrodes or metal fines that can ingress a battery during manufacturing. The elastic modulus is determined from the unloading portion of a load–unload cycle. The hardness is calculated from the residual indentation area left after plastic deformation of a material beyond its elastic limit. It is intuitively clear that a separator's ability to resist penetration is described both by stiffness and hardness, since the former quantifies its ability to oppose elastic deformation and the latter that of opposing permanent deformation. We report herein on nanoindentation experiments performed on several polymeric and ceramic-enhanced separators using a Berkovich tip, to estimate their mechanical properties (elastic modulus and Martens hardness) at room temperature (25 °C). We also propose nanoindentation for quantifying and ranking the puncture resistance of LIB separators, which can also be used as a quality-control tool for their uniformity.

2. Experimental

Nanoindentation experiments were performed with an MTS NanoIndenter XP instrument and a Berkovich tip (equilateral triangular pyramid with square base) having a 50 μm side on its base, a 1:7 height-to-side aspect ratio and a 0.05 μm radius at the apex. For each sample, indentations were performed at 25 °C on a 5 × 5 matrix of points with 500 μm spacings, by successively applying (at each spatial location) five successive load–unload cycles with increasing maximum loads and a 90% unload in each cycle (see Fig. 1). The maximum applied load during the fifth load–unload cycle was 9.8 mN. Measurements on each sample were bracketed by measurements on silica, performed as calibration checks and to remove debris from the indenter tip. The elastic modulus and hardness were determined from the unloading curves with the Oliver-Pharr method [6,7] for several polymeric and ceramic-enhanced separators (see Table 1 for composition and properties) using the data analysis software package provided with the MTS instrument. The polymeric separators were (1) two commercial single layer polypropylene separators (PP1 and PP2), (2) a commercial polypropylene–polyethylene–polypropylene trilayer

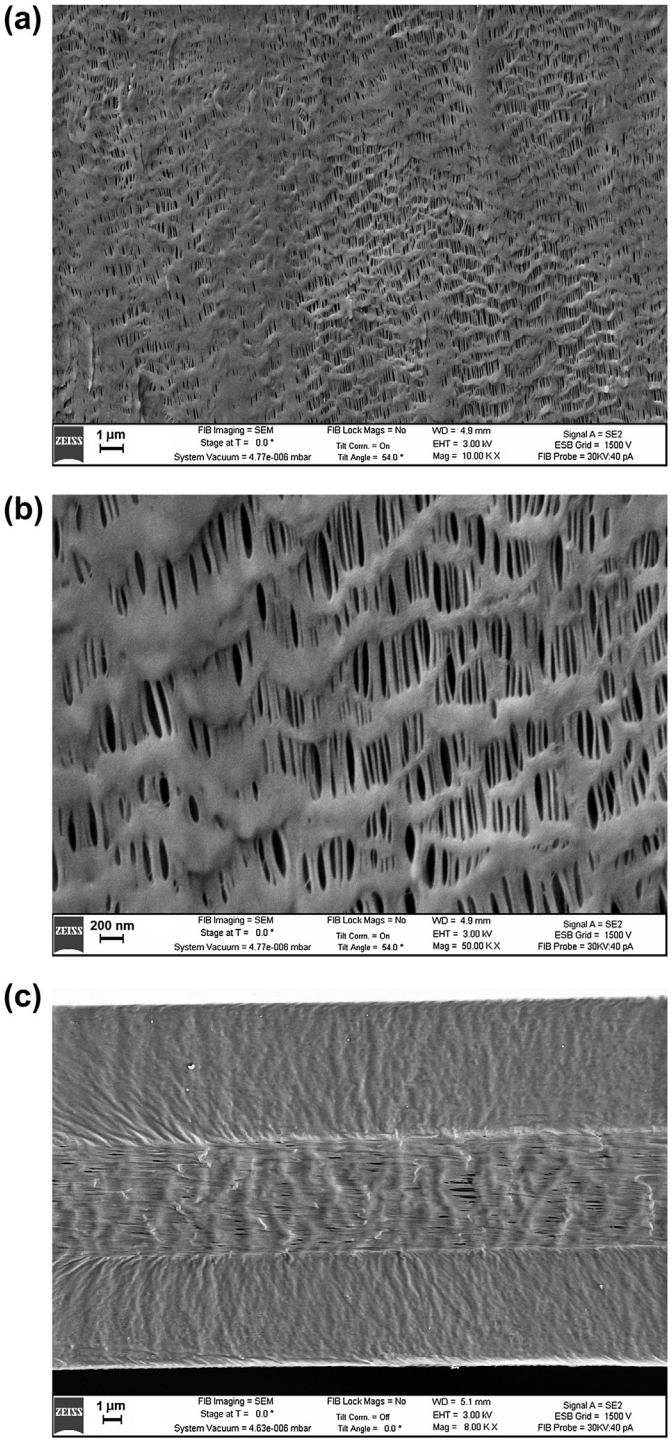

Fig. 3. SEM micrographs of the trilayer PP–PE–PP separator: (a) surface at low magnification; (b) surface at high magnification; (c) cross-section.

(PP–PE–PP), and (3) an experimental polytetrafluoroethylene (PTFE) separator. The ceramic-enhanced separators were made of (1) woven polyethylene terephthalate, PET, enhanced with corundum Al_2O_3 and fumed SiO_2, (2) a commercial PP–PE–PP trilayer coated with Al_2O_3 on both sides, and (3) an experimental composite material consisting of UHMWPE and fumed Al_2O_3 with a polymer-filler ratio of 1:2, in the as-prepared and heat-treated state. The separator morphology was investigated with a Carl Zeiss SMT NVision scanning electron microscope (SEM) operating at 3 kV. Cross-sectioned specimens were prepared at room with a diamond knife microtome. All specimens were sputter coated with an Au–Pd alloy to improve image quality.

3. Results and discussion

SEM micrographs for PP1 and PP–PE–PP are shown in Figs. 2 and 3, respectively. The pores in both separators were produced with a dry process by deformation induced crazing (uniaxial stretching), which results in shear bands that yield fibrils giving rise to well-defined elliptical pores oriented parallel to the deformation direction. Pores in the single layer PP1 are larger and have a more uniform distribution than in the PP–PE–PP trilayer. Pore sizes were 0.60 × 0.10 μm for PP1 and 0.40 × 0.04 μm for PP–PE–PP. The trilayer construction is evident in the cross-section from Fig. 3(c), with each layer of equal thickness.

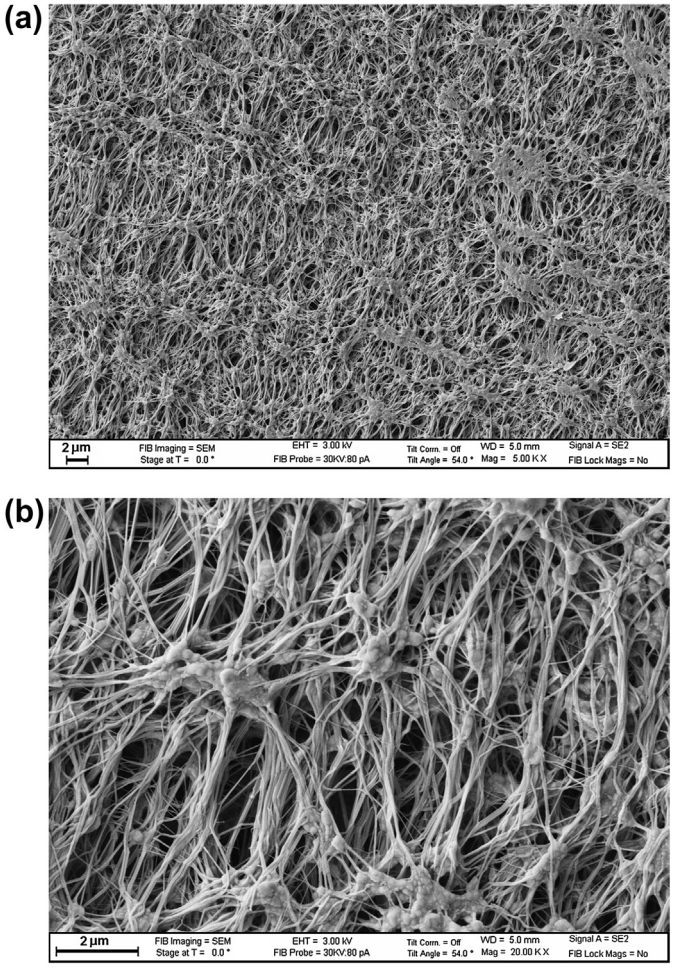

Fig. 4. SEM micrographs of the PTFE separator: (a) surface at low magnification; (b) surface at high magnification.

SEM micrographs for PTFE are shown in Fig. 4. This separator has fibrils and nodes typical for expanded PTFE. Pore sizes range up to 2 μm, the largest among all examined separators.

The SEM images for the ceramic-enhanced PET separator show large holes (Fig. 5a). Higher magnification reveals a very lose ceramic coating (Fig. 5b) and holes with 5–10 μm cross-sectional dimensions. A woven fiber construction reinforced and coated with ceramic powders can be seen quite clearly in the cross-section

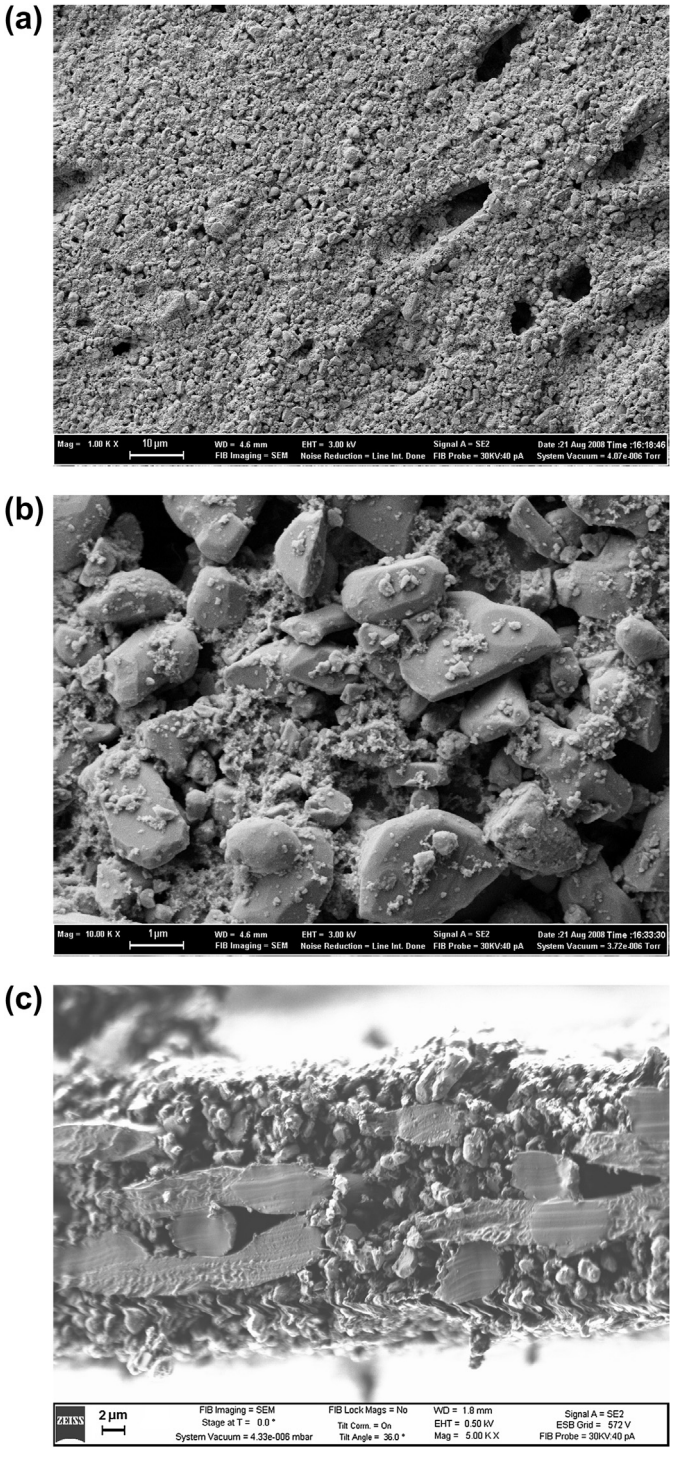

Fig. 5. SEM micrographs of the composite separator made of woven PET, corundum Al_2O_3 and fumed SiO_2 ceramics: (a) surface at low magnification; (b) surface at high magnification; (c) cross-section.

SEM micrograph from Fig. 5c, with fibers having ~4 μm diameters. The surface comprises oxide particles of two sizes: large particles made of corundum (Al_2O_3), approximately 1 μm in cross dimension, and small particles with diameters less than 0.10 μm, made of fumed silicon dioxide (SiO_2).

The ceramic-coated PP–PE–PP separator has the most complex construction (see Fig. 6a–d). It is an assembly of five layers, as seen in the cross-section SEM (Fig. 6c) and optical (Fig. 6d) micrographs. The two outer layers are made of ceramic particles and organic binder (Fig. 6c). (The roughness of the two outer ceramic containing layers is a sample preparation artifact.) The ceramic particles are less than 1 μm in cross-sectional dimension (Fig. 6b). The center three layers represent the PP–PE–PP trilayer.

Fig. 7(a)–(c) shows SEM micrographs for the as-prepared Al_2O_3 filled UHMWPE separator. Fumed Al_2O_3 particles on the surface appear in the bright regions as small agglomerated clusters (Fig. 7a). The lamellar-and-extended-needle (a.k.a. shish-kebab) structure (Fig. 7b) stems from the fabrication process. Pores are formed by the space between the lamellar and the extended needle structures. Heat-treatment of the Al_2O_3 filled UHMWPE separator (Fig. 8a–c) leads to in a loss in definition for the shish-kebab structure and also increased cross-linking (Fig. 8b). The heat-treated material has fewer but larger pores than the as-prepared material. The pore structure is uniform throughout the cross-section in both separators (Figs. 7c and 8c).

An examination of the face-on SEM micrographs at low magnification reveals much more uniform surface features for PP1 (Fig. 2a), PTFE (Fig. 4a) and Al_2O_3 filled UHMWPE (Figs. 7a and 8a) than for PP–PE–PP (Fig. 3a), ceramic-enhanced PET (Fig. 5a) and ceramic-enhanced PP–PE–PP (Fig. 6a). This difference in surface uniformity may (in part) stem from the complexity of the processing involved in making the latter three separators.

Fig. 9 displays load vs. displacement curves for seven of the separators tested in our work. Note that all load–unload curves exhibit hysteresis as well as creep, typical of the visco-elasto-plastic behavior of polymers. Averages values for the maximum indenter displacements range from 3 μm and 5 μm in the bimodal distribution for as-prepared Al_2O_3 filled UHMWPE to 18 μm for PTFE.

The elastic modulus and hardness for each sample are displayed in Figs. 10–12 and listed in Table 3. Note that conventional nano-indentation methods for calculating the modulus of elasticity based on the unloading curve are limited to linear, isotropic and homogenous materials. These assumptions are clearly violated by the materials investigated in the present work. The separators are anisotropic inhomogeneous media (see the SEM micrographs from Figs. 2–8). Furthermore, the data from Fig. 9 show that the mechanical response of these materials is nonlinear and exhibits hysteresis as well as creep. These well-founded objections notwithstanding, we used the Oliver-Pharr method as a means for achieving a first-order quantitative comparison of separator

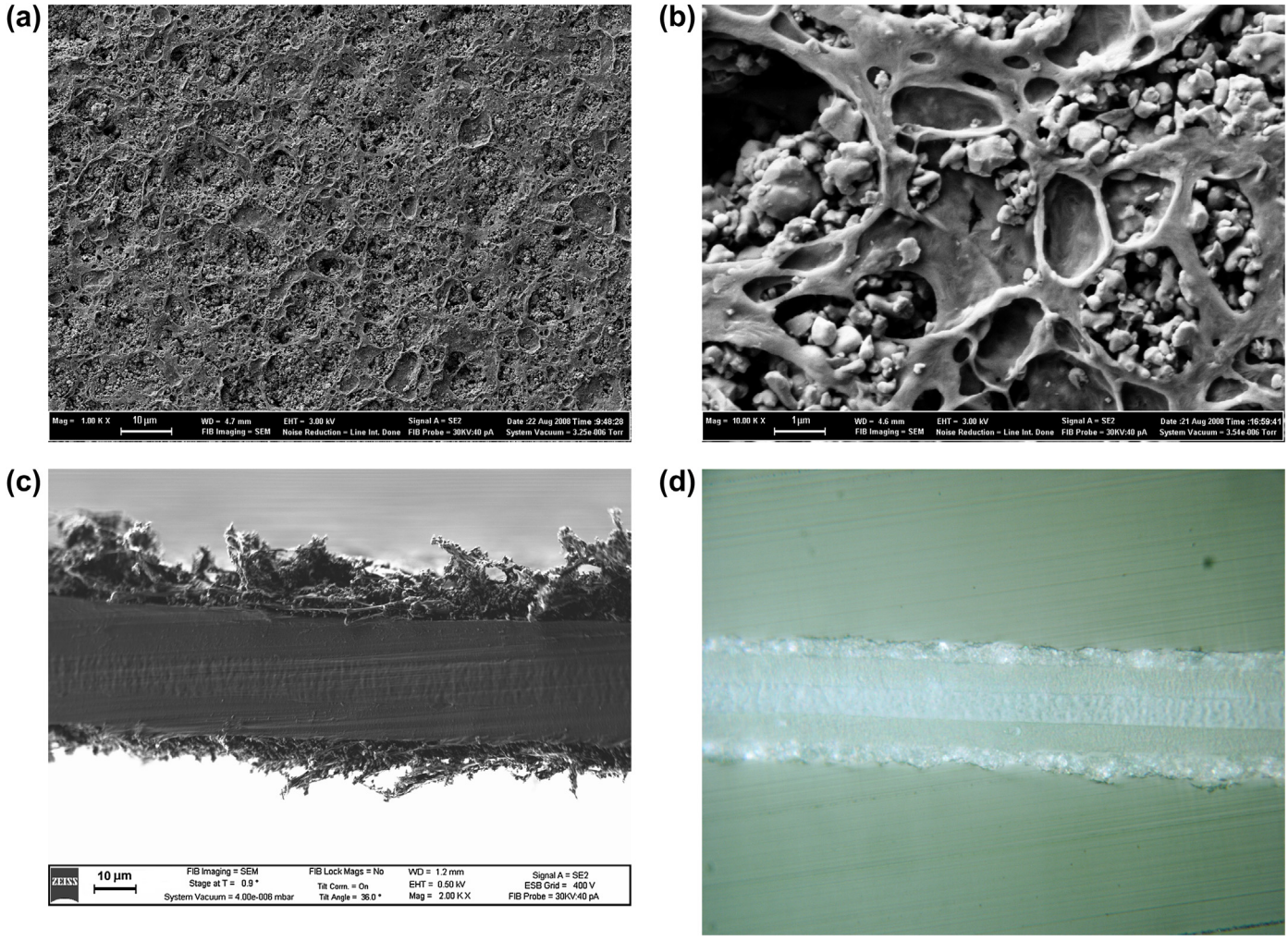

Fig. 6. SEM micrographs of the Al_2O_3-coated PP–PE–PP separator: (a) surface at low magnification; (b) surface at high magnification; (c) cross-section; (d) optical micrograph of the separator cross-section.

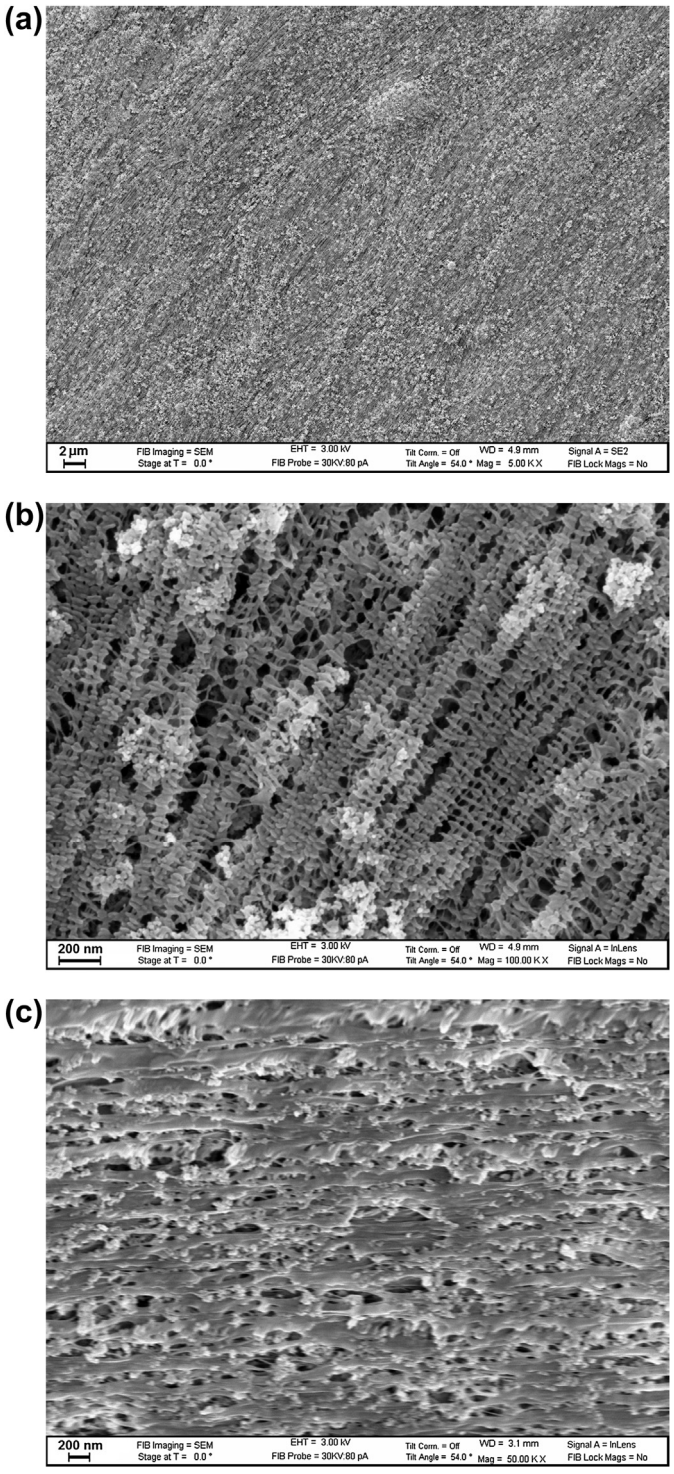

Fig. 7. SEM micrographs of as-prepared composite UHMWPE plus fumed Al_2O_3 separator: (a) surface at low magnification; (b) surface at high magnification; (c) cross-section.

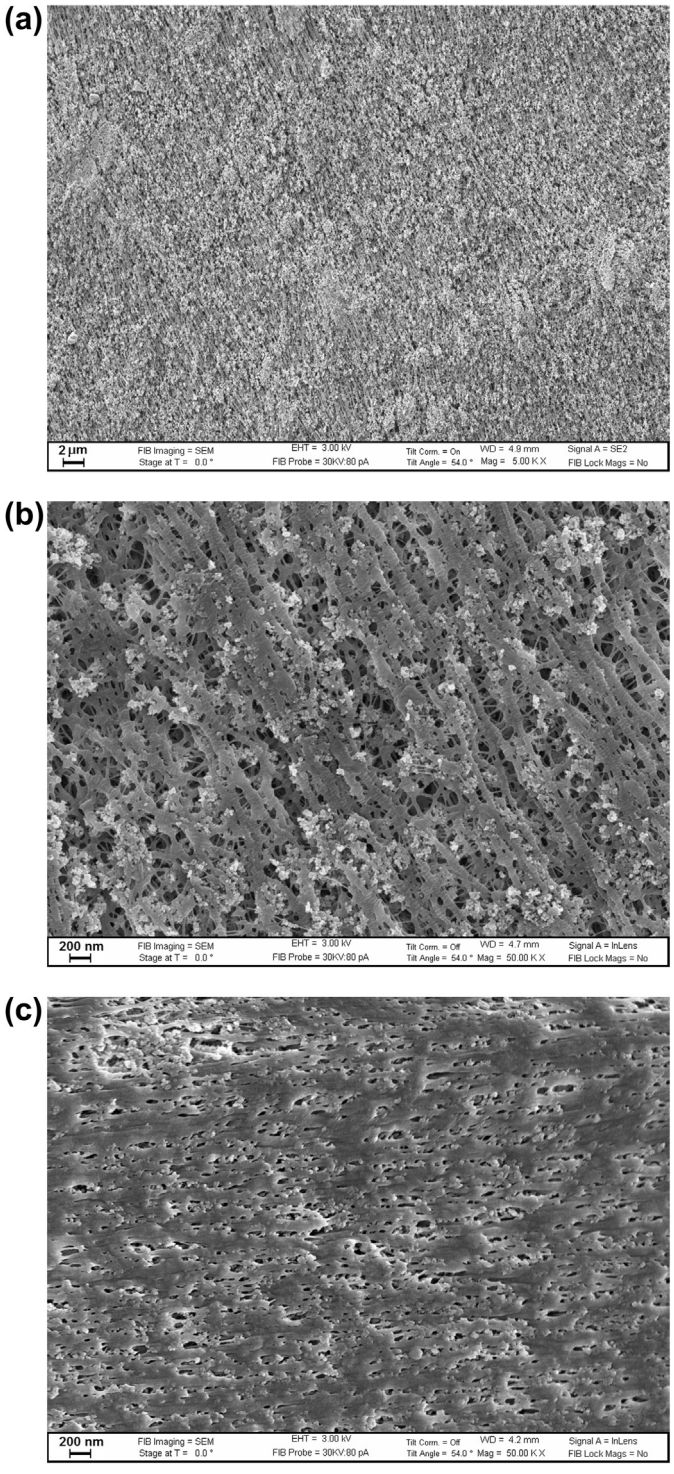

Fig. 8. SEM micrographs of heat-treated composite UHMWPE plus fumed Al_2O_3 separator: (a) surface at low magnification; (b) surface at high magnification; (c) cross-section.

properties and attempted to quantified the degree of nonlinearity by performing five load–unload cycles with increasing maximum loads for each point in the 5 × 5 sample matrix. Fig. 1 displays the temporal evolution of the load applied on the samples, showing five consecutive load–unload segments, each with increasingly higher load change rates, ranging from 0.038 mN s^{-1} to 0.62 mN s^{-1}. The maximum load for each of the five load–unload segments, together with the respective load change rates is listed in Table 2. The data from Fig. 10 clearly show that the elastic modulus is load dependent. The hardness, on the other hand, is a much weaker function of applied load, as seen from Fig. 11. Given that in our experiments both the maximum applied load and the load change rate varied with each load–unload segment (see Fig. 1 and Table 2), it is legitimate to ask whether the variations in the elastic modulus and hardness seen in Figs. 10 and 11, respectively, are due to changes in maximum load and/or load change rate. We have

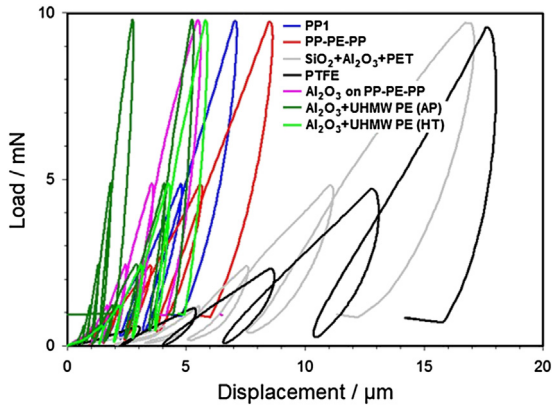

Fig. 9. Load vs. displacement curves for the separators tested in this work, corresponding to the array averaged nanoindenter displacement for each material. All load–unload curves exhibit hysteresis typical of the visco-elasto-plastic behavior of polymers. The maximum displacement is highest for PTFE (18 μm) and smallest for the as-prepared Al_2O_3 filled UHMWPE (3 μm). Note the bi-modal distribution for the latter separator.

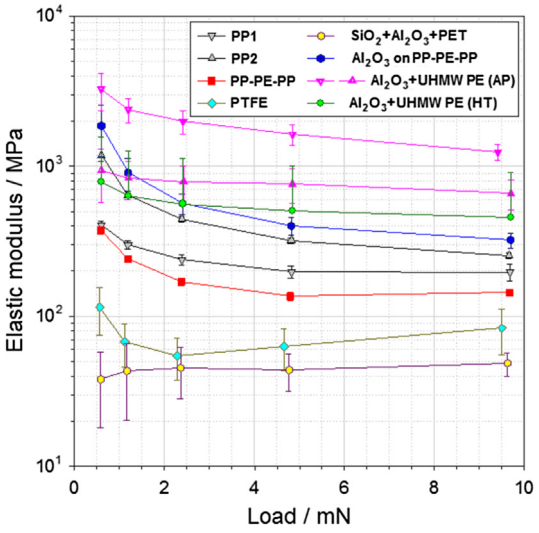

Fig. 10. Average elastic modulus vs. load for the separators from the present work.

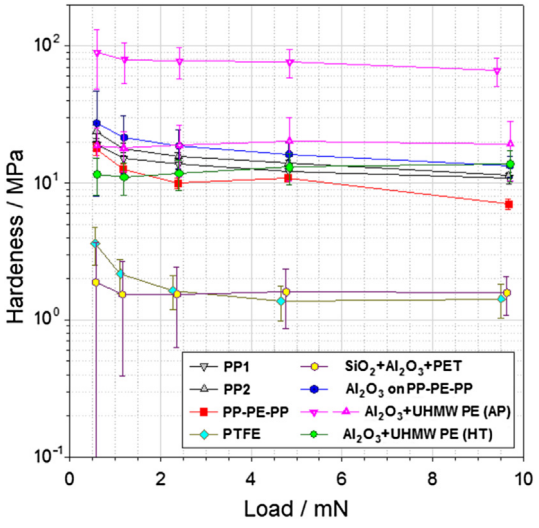

Fig. 11. Average hardness vs. load for the separators from the present work.

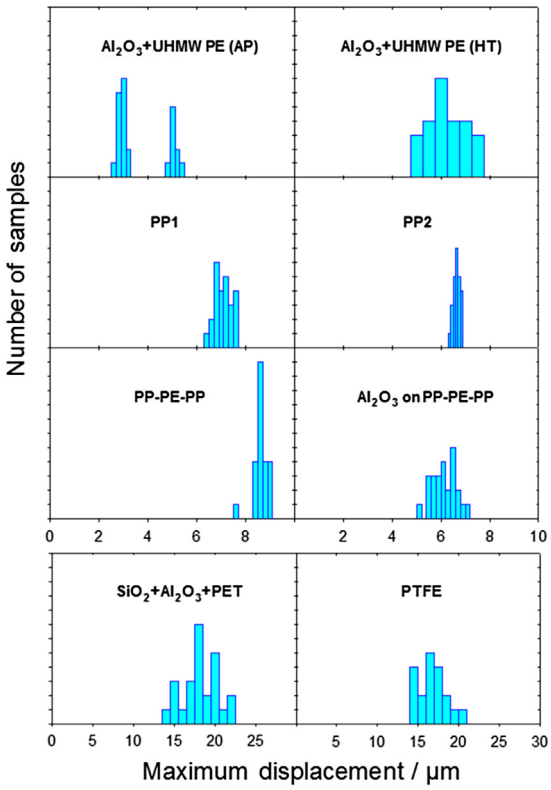

Fig. 12. Distribution of indentation depths in the 5 × 5 measurement arrays for the tested separators. Each ordinate division represents one sample. Note the change in the scale of the *x*-axis in the two lowest panels.

examined this issue extensively and concluded that the observed changes are due primarily to changes in maximum applied load when load change rates vary by more than two orders of magnitude.

Fig. 10 shows that array-averaged elastic modulus values range from 40 MPa for the composite $SiO_2 + Al_2O_3 + PET$ separator to 3 GPa for the as-prepared composite Al_2O_3 + UHMWPE separator. Furthermore, the separators rank in the following order by elastic modulus (for loads greater than 2 mN): composite $SiO_2 + Al_2O_3 + PET$ composite ~ PTFE ≪ PP–PE–PP < PP1 < PP2 < Al_2O_3 coated PP–PE–PP < heat-treated Al_2O_3 filled UHMWPE < as-prepared Al_2O_3 filled UHMWPE. The composite Al_2O_3 + UHMWPE and the Al_2O_3 coated PP–PE–PP separators have the highest modulus values (between 500 MPa to 3 GPa). The single layers PP1 and PP2, and also the trilayer PP–PE–PP separator have intermediate values (from 150 to 2 GPa). The PTFE and the Al_2O_3 + SiO_2 enhanced PET separators have the lowest values (from 40 to 100 MPa). Note that the as-prepared Al_2O_3 + UHMWPE separator exhibits a bi-modal distribution in load–unload curves (see Figs. 9 and 12), which disappears subsequent to heat-treatment above 100 °C. While Al_2O_3 filled UHMWPE and Al_2O_3 PP–PE–PP separators have a higher elastic modulus than the unfilled separators, the elastic modulus of the ceramic-enhanced PET separator is significantly lower than that of most polymeric separators and practically identical to that of the PTFE separator. Note also that the Al_2O_3 filled UHMWPE separators have a higher elastic modulus than all other separators, even though their porosity

Table 2
Maximum loads on the samples during the five load–unload segments of the nanoindentation tests and the corresponding load change rates.

Maximum load (mN)	0.60	1.20	2.5	5	10
Load change rate (mN s^{-1})	0.04	0.08	0.15	0.31	0.62

Table 3
Nanoindentation test results.

No.	Composition	Elastic modulus, MPa	Hardness, MPa	Average max. displacement, μm	Average max. displacement, % of thickness
1	PP1	197 ± 24 (12%)	10.9 ± 1.1 (10%)	7.00 ± 0.35	28
2	PP2	254 ± 12 (5%)	11.3 ± 0.5 (4%)	6.64 ± 0.14	25
3	PP–PE–PP	144 ± 7 (5%)	7.0 ± 0.6 (8%)	8.54 ± 0.29	40
4	PTFE	83 ± 28 (34%)	1.4 ± 0.4 (28%)	17.9 ± 2.8	78
5	SiO_2 + Al_2O_3 + PET	49 ± 9 (18%)	1.6 ± 0.5 (31%)	17.7 ± 2.3	59
6	Al_2O_3 coated PP–PE–PP	322 ± 37 (12%)	13 ± 2 (17%)	6.1 ± 0.5	25
7	Al_2O_3 + UHMWPE (AP)	1240 ± 149 (12%)	66 ± 16 (24%)	2.8 ± 0.3	4.6
		660 ± 146 (22%)	19 ± 9 (47%)	5.2 ± 1.1	1.8
8	Al_2O_3 + UHMWPE (HT)	456 ± 149 (33%)	14 ± 4 (26%)	6.0 ± 0.8	1.9

exceeds that of the polymeric separators with similar mechanical properties from the present study by factors ranging from 1.4 to 2.3 (see Table 1).

Fig. 11 displays array averaged hardness values as function of load. The data cluster into three readily discernible sets: (1) a bimodal distribution for as-prepared Al_2O_3 filled UHMWPE, with a low value around 20 MPa and high a value ranging from 70 to 90 MPa; (2) unimodal distributions for PP1, PP2, PP–PE–PP, ceramic coated PP–PE–PP and heat-treated Al_2O_3 filled UHMWPE, with average values of 7–30 MPa; (3) unimodal distributions for the PTFE and the Al_2O_3 + SiO_2 enhanced PET separators, with the lowest and practically identical average values, ranging from 1.5 MPa and 4 MPa. Note that the heat-treated Al_2O_3 filled UHMWPE separator has practically the same hardness as the PP1, PP2, or Al_2O_3 coated PP–PE–PP separators, even though its 80% porosity is much higher than the 34–50% values for the other four separators. Both the results for the elastic modulus and hardness clearly show that material composition (ceramic–polymeric composite vs. purely polymeric) and also fabrication methods (UHMW-based composite vs. PET-based composite) can play a more important role than the void-to-matrix ratio (i.e. membrane porosity) in determining the mechanical properties of a separator.

Statistical distributions of maximum indentation depths over the 5 × 5 measurement arrays for all separators are shown in Fig. 12. Note that, except for as-prepared Al_2O_3 + UHMWPE, all distributions are unimodal. The as-prepared Al_2O_3 filled UHMWPE separator exhibits a bimodal distribution with values clustered in two narrow intervals centered on average indentation depths that are lower than all others, which is consistent with its higher elastic modulus and hardness (see Figs. 10 and 11). Upon annealing, the distribution becomes unimodal and broadens, with an increase in depth, consistent with softening of the film. The penetration depths for separators with unimodal distributions cluster in two groups: (1) PP1, PP2, PP–PE–PP, SiO_2 + Al_2O_3 filled UHMWPE and Al_2O_3 coated PP–PE–PP, with values in the range of 6–9 μm; (2) PTFE and SiO_2 + Al_2O_3 + PET composite, with values in the range of 15–20 μm. Among the tested separators, the PP2, PP–PE–PP and as-prepared Al_2O_3 filled Al_2O_3 UHMWPE separators exhibited the narrowest distributions of penetration depths, while the PTFE and SiO_2 + Al_2O_3 + PET separators had the widest distributions. This exemplifies how nanoindentation can be used as a quality-control tool for separators, both during product development and in production, to determine the in-plane uniformity of properties.

4. Conclusion and directions for future work

The elastic modulus values for the separators tested in the present work range from 40 MPa for the ceramic-enhanced PET separator to 3 GPa for the as-prepared Al_2O_3 filled UHMWPE separator, and rank in the following order: ceramic-enhanced PET < PTFE ≪ PP–EP–PP < PP1 < PP2 < Al_2O_3 coated PP–PE–PP < heat-treated Al_2O_3 filled UHMWPE < as-prepared Al_2O_3 filled UHMWPE. The PTFE and ceramic-enhanced PET separators have both the lowest elastic modulus and lowest hardness values. Their hardness is lower by more than one order of magnitude compared to the other tested separators, very likely indicative of a poor puncture resistance. The Al_2O_3 filled UHMWPE separators, with porosity of 80% have a higher elastic modulus than, and the same hardness as, the PP1, PP2, PP–PE–PP and ceramic coated PP–PE–PP separators, which have significant lower porosity (ranging from 34 to 50%). Our results clearly indicate that, while the use of ceramic material (either as filler or coating) can enhance the mechanical properties of separators, this is not necessarily always the case, as these properties are highly dependent on the morphology of the ceramic–polymer composite and on processing conditions. Depending on details of composition and processing, the elastic modulus of the separators from the present study varies by a factor of 30–100 over the range of loads applied in our experiments, while the hardness values are only a weak function of load and vary by a factor of 40–70. The data for the as-prepared and heat-treated Al_2O_3 filled UHMWPE separators illustrate the strong effect of thermal history on the mechanical properties and morphology of ceramic-enhanced separators.

The present study was preliminary in nature, aiming to explore the utility of nanoindentation for the context of Li-ion battery separators. We remind the reader that the assumptions of linearity and medium homogeneity, inherent in the Oliver-Pharr analysis, are not valid in the present cases. This caveat notwithstanding, our analysis provides a means assessing the uniformity of separators and quantifying (albeit in a first approximation) the mechanical properties for the purpose of ranking. The large scatter in parameter values (as evidenced by standard deviations of 20–30% for all but three of the separators from the present study) provides another justification for our simplified analysis, as the elastic modulus and hardness values determined with a more elaborate model that accounts for viscous effects are likely to fall within these ranges of variation.

Future studies should include the investigation of the viscoelastic response of the separators, to more comprehensively account for separator properties. A systematic investigation of the mechanical properties as a function of temperature is also needed in order to quantify the mechanical properties of separators under conditions of thermal abuse. The present study investigated the mechanical properties that are relevant to the puncture resistance of separators in prismatic cells. Abrasion resistance measurements are necessary to quantify the ability of separators to prevent battery shorting by loose conductive particles in spirally wound cylindrical cells. The present

work was performed on as-fabricated dry separators before their use in a battery. It is desirable to determine the mechanical properties of electrolyte filled separators, i.e., under conditions that better approximate those existing in a battery. Finally, it is recommended to determine the mechanical properties of separators after their use in batteries, to investigate their stability under normal battery use.

Acknowledgments

We thank Dr. Mark Verbrugge for providing inspiration, encouragement, and support for the present work. We also acknowledge Dr. Gregory MacLean and Mr. Harshad Tataria for insightful discussions and comments.

References

[1] D. Doughty, in: Proceedings of the First International Symposium on Large Lithium Ion Battery Technology and Application, Honolulu, HI, June 13–15, 2005.
[2] E.P. Roth, in: Proceedings of Lithium Mobile Power Conference, San Diego, CA, 2007.
[3] ASTM F1306-90, Standard Test Method for Slow Rate Penetration Resistance of Flexible Barrier Films and Laminates, 2008.
[4] W.J. Schell, Z. Zhang, in: The Fourteenth Annual Battery Conference on Applications and Advances, IEEE, New York, 1999, pp. 161–169.
[5] P. Arora, Z. Zhang, Chem. Rev. 104 (2004) 4419–4462.
[6] X. Xiao, W. Wu, X. Huang, H. Kia, J. Power Sources 195 (2010) 7649–7660.
[7] D. Shi, X. Xiao, X. Huang, H. Kia, 196 (2011) 8129–8139.
[8] A. Sheidaei, X. Xiao, W. Wu, J. Hilt, J. Power Sources 196 (2011) 8228–8234.
[9] C. Peabody, C.W. Arnold, J. Power Sources 196 (2011) 8147–8153.
[10] J. Cannarella, C.W. Arnold, J. Power Sources 226 (2013) 149–155.
[11] W.C. Oliver, G.M. Pharr, J. Mater. Res. 7 (1992) 1564–1580.
[12] W.C. Oliver, G.M. Pharr, J. Mater. Res. 19 (2004) 3–20.